Sci. Rep. Kanazawa Univ.
Vol. 64, pp. 1–13, 2020

ARTICLES

Electronic structure investigation of spinel $NiCo_2O_4$ from quasi-particle self-consistent GW method

Hasan AL RASYID,*[1,2] Masao OBATA,[1,3] Indra PARDEDE,[3,4] Marleni WIRMAS,[1]

Takao KOTANI,[5] Tatsuki ODA[1,3]

[1]Graduate School of Natural Science and Technology, Kanazawa University
Kanazawa, 920-1192, Japan
[2]Faculty of Mathematics and Natural Sciences, Institut Teknologi Bandung
Bandung, 40132, Indonesia
[3]Institute of Science and Engineering, Kanazawa University
Kanazawa, 920-1192, Japan
[4]Department of Physics, Institut Teknologi Sumatera (ITERA)
Lampung Selatan, 35365, Indonesia
[5]Department of Applied Mathematics and Physics, Tottori University
Tottori, 680-8552, Japan

(Receieved June 19, 2020 and accepted in revised form August 12, 2020)

Abstract Quasi-particle self-consistent GW (QSGW) electronic structure calculation was performed in three spinel structures of ternary magnetic compound $NiCo_2O_4$, i.e. normal spinel and two of inverse spinel structures (Types A and B). The QSGW method is state-of-the-art on electronic structure investigation without using any empirical parameter. The results were also compared with those from the density functional theory (DFT) based on generalized gradient approximation (GGA). Half-metallicity was observed in all cases investigated, where the band energy gap appears in the majority spin state. The QSGW indicated that the gap is larger than that of the corresponding GGA case. The QSGW may yield more localized *d*-orbitals, compared with those from the GGA. Based on the projected density of states (PDOS) analysis, Co atoms of the octahedral site [Co(oct)] were found to be a non-magnetic/weak magnetic configuration (low spin state) among them, resulting in a negligible contribution to the total magnetization. The largest contribution to the total magnetization is provided by Co atoms of tetrahedral [Co(tet)] site (high spin state). The QSGW indicated the difference of octahedral crystal fields on the different cation sites of Co(oct) and Ni(oct). The electronic states near the Fermi level consist mainly of Co(tet) 3d e_g-orbitals. In the normal and inverse (type A) spinels, the Fermi level crosses the states with the DOS having a large sharp peak, implying instability of the electronic structure. The results of QSGW were discussed by comparing with those of one-shot GW and other methods.

Keywords. QSGW method, DFT method, *ab-initio* electronic structure, spinel, nickel cobaltite.

*Corresponding author Email: hasanalrasyid.har@gmail.com

1 Introduction

Oxygen reduction reaction (ORR) is one of the most basic reactions that construct many complex reactions such as energy generation (fuel cell), weathering of materials, and most of the biological processes [1]. One of the main interests of this reaction focused on its role in the oxygen electrode used in electrical-power related systems, i.e. metal-air batteries and fuel cells. From this point of view, being an abundantly available transitional metal oxide, Nickel cobaltite, $NiCo_2O_4$, shows many advantages, compared to already available alternatives. In catalysis, $NiCo_2O_4$ has a role as a heterogeneous catalyst with the reaction of ORR. However, the mechanism of ORR on metal surfaces remains unclear. $NiCo_2O_4$ indicates a half-metallic property, according to low field magnetoresistance (LFMR) measurements [2]. Nickel cobaltite is also reported to be half-metallic with -19.1% low-field magnetoresistance at 0.5 T and -50% at 9 T (both measured at 2 K) [2]. Combined with its high Curie temperature (295K [3], 350K [4]), these properties made nickel cobaltite into a good candidate as spintronic materials. One can easily tune its electrical and magnetic properties by varying the crystal growth temperature and oxygen pressure [5]. The interest on $NiCo_2O_4$ mainly comes from its abundance and its potential use, as spintronics application, as well as an alternative electrode used in electrical-power related systems, i.e. metal-air batteries and fuel cells. $NiCo_2O_4$ is one of the promising materials to be used in applications of catalysis and spintronics.

$NiCo_2O_4$ is a ferrimagnet [4, 6] and one candidate of novel materials that could be engineered in many ways to exhibit different properties. By utilizing temperature growth of less than 450°C, one can acquire metallic-ferrimagnetic $NiCo_2O_4$ thin film. On the contrary, with more than 450°C, we would acquire thin film as a non-magnetic insulator [7]. This uniqueness is believed to come from the competition between double exchange interaction among cations with different charges and superexchange interaction among those with the same charges [3].

An electronic structure investigation from a theoretical approach was reported in the work combined with the experimental measurement [8]. The authors have used a modified Becke-Jonson formula in the exchange-correlation function based on local spin density approximation (mBJ-LDA). It reported large energy gaps of around $3-4$ eV in majority spin states between the valence and conduction bands, and the result indicated a half-metallic property. The properties of electronic structure, such as large energy gap, have not been validated yet and the details on the electronic structure are not so clear that they are self-consistently understood with the properties of catalysis. The successive theoretical approach, namely the LDA+U approach, introduced an on-site Coulomb parameter of the Hubbard model, U_{eff}, to the cation sites [2, 5]. The results of the spin-polarized density of states indicated a half-metallic property with an energy gap in the majority-spin state of about 1.3 eV. The analysis of atomic and orbital projections revealed electrons of the Ni(Oct) and Co(Tet) orbitals hybridized with O at the Fermi level. The obtained pictures on electronic and magnetic structures at the Fermi level may be based on the understanding or interpretation of many complicated experimental observations [2, 5]. This means that one can get some satisfaction from such a theoretical approach to its half-metalicity. However, in those approaches, the empirical parameters were used for the U_{eff} on Ni and Co sites which were introduced as Fe spinel oxides [9]. The semiconducting/insulating property of $NiCo_2O_4$ has not been discussed from theoretical electronic structure results.

We have theoretically investigated the electronic and magnetic properties of bulk $NiCo_2O_4$ to understand its basic features. In our theoretical investigation, quasi-particle self-consistent GW (QSGW) calculations [10, 11, 12] were performed in normal and inverse spinels of $NiCo_2O_4$. This method does not employ any empirical parameters such as U_{eff}. This feature indicated a lot

Table 1: Configurations of tetragonal and octahedral sites for X and Y elements in the spinel structure XY_2O_4. The numbers in parentheses are the number of atoms per formula unit.

system	tetrahedral site (2)	octahedral site (4)
Normal	X(2)	Y(4)
Inverse type A	X(1),Y(1)	X(1), Y(3)
Inverse type B	Y(2)	X(2), Y(2)

of advancements in the electronic structure analyses of semiconducting and insulating materials. The QSGW method enables the calculation of metallic electronic structures. Such an advantage may be useful for a wide range of materials in the advanced methods beyond the density functional theory (DFT) [13] approach. The performance of QSGW beyond DFT in improving the electronic structure of semiconductors has been well known already [11]. The recent progress has reached to a group of materials for power electronics [14, 15] and a group of surfaces [16]. We can find more data about applicability on its performance on wider sets of materials, i.e. half-metallic, magnetic, and metallic materials.

The half-metallic property was found on all the results of $NiCo_2O_4$ and the metallicity is associated mainly with the 3d orbitals on tetrahedral Co(tet) in the minority spin state. The QSGW investigation revealed that the Ni 3d components at the octahedral site are largely suppressed at the Fermi level by a mixed-valence feature with the hybridization with O 2p orbital.

2 Crystal structure and computation method

2.1 Normal and inverse spinel structures

Spinel materials or their family are usually presented as a chemical formula XY_2O_4, where X and Y are cationic elements. For the cationic elements, there are two distinguishable atomic sites. They have tetrahedral and octahedral symmetries, called tetrahedral and octahedral sites, respectively. There are 2 tetrahedral sites and 4 octahedral sites in a primitive unit cell (two formula units). In the normal spinel, all of X occupies the tetragonal site and all of Y at the octahedral site. In inverse spinel structure, X and Y atoms are interchanged with each other between the tetrahedral and octahedral sites. As in the previous work of $NiCo_2O_4$ [7], we considered two types of inverse spinel, called Types A and B (inverse A and inverse B). The configurations of tetrahedral and octahedral sites for X and Y elements are presented in Table 1.

The crystal structure of the normal spinel belongs to a faced-centered cubic structure with the space group of No. 227. In the case of $NiCo_2O_4$, its structure was reported to have an inverse spinel structure [6]. We calculated normal and two inverse spinel structures of $NiCo_2O_4$. The normal and inverse spinel structures (inverse A and inverse B) are presented in Figure 1. Silwal *et al.* [7] suggested that the inverse B configuration has a higher tendency to happen rather than inverse A configuration. Our discussion in this paper particularly focused on the inverse type B.

Figure 2 picks up atomic configurations at the tetrahedral and octahedral sites in the spinel structure. Each cation atom is surrounded by four or eight oxygen atoms depending on these sites. Oxygen imposes a strong crystal field at the cation site. As a consequence of such crystal field, the five energy levels of 3d orbital will split into two kinds of levels denoted as t_{2g}(3 levels) and e_g(two levels). For the tetrahedral site surrounded by negatively charged oxygen, the t_{2g} levels are lowered and those of e_g are raised. In the octahedral site, this level arrangement is reversed. The

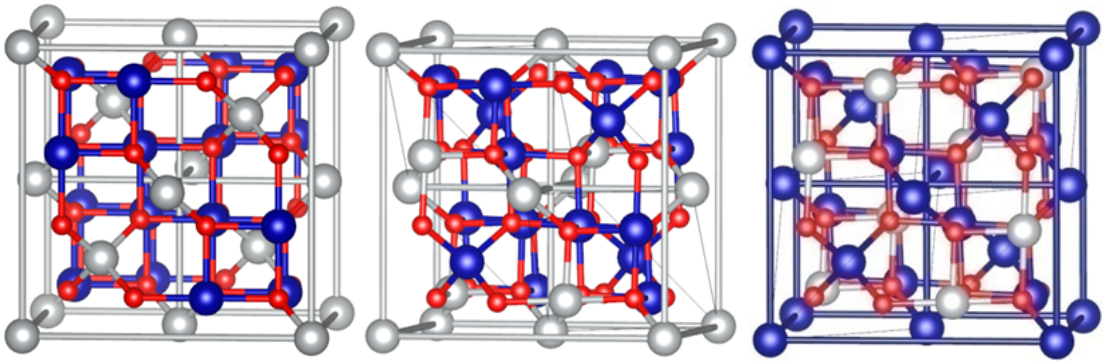

Figure 1: Three spinel structures of $NiCo_2O_4$. From left to right, they indicate spinels of normal, inverse type A, and inverse type B. Ni, Co, and O atoms are represented by silver, blue, and red color respectively.

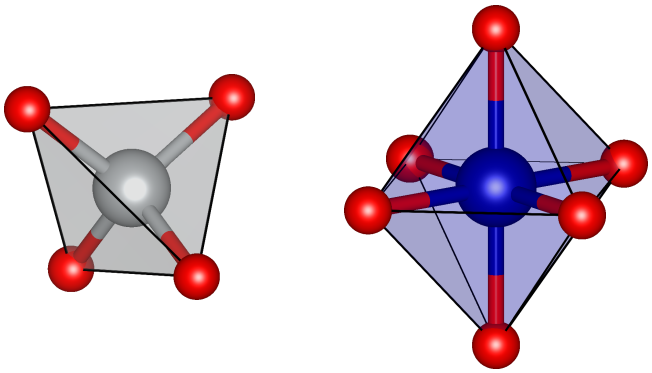

Figure 2: Atomic configurations of tetrahedral (left) and octahedral (right) sites, respectively. Silver or blue balls denote a cation atom and red balls denote oxygen atom.

energy width of this splitting may indicate the degree of the crystal field.

We investigated the optimized structure of the lattice parameter a and internal parameter u using the house-package of DFT(GGA) code [17] for the normal spinel structure of $NiCo_2O_4$. As u increases, the oxygen tetrahedron around the cation of the tetrahedral site expands, resulting in an elongation of the cation-oxygen bond. They were determined to be $a = 8.115$ Å and $u = 0.3881$. The former was in agreement with the experimental values. Thus, we decided to use the set of experimental values in our further research. Indeed, we took the experimental values of $a = 8.114$ Å and $u = 0.3833$ [6, 18]. The difference (δu) between two internal parameters presented above corresponds to an oxygen atomic distortion of 0.07 Å ($=\sqrt{3}a\ \delta u$). This is much smaller than a standard bond length of Ni-oxide (0.4%) [6].

2.2 Calculation procedure

In the QSGW calculation, the energy level (ε_i and $|\Psi_i\rangle$: eigenvalue and eigenstate) of quasi-particle (QP) is obtained by solving the equation

$$\left[-\frac{\hbar^2}{2m}\nabla^2 + V_{\text{ext}} + V_{\text{H}} + V_{\text{xc}}\right]|\Psi_i\rangle = \varepsilon_i|\Psi_i\rangle, \tag{2.1}$$

where V_{ext}, V_{H}, and V_{xc} are the potentials from nuclei, the electrostatic potential from electrons, and exchange-correlation potential, respectively. V_{xc} is self-consistently evaluated from the following formula:

$$V_{\text{xc}} = \frac{1}{2} \sum_{i,j} |\Psi_i\rangle \left[\text{Re}\{\Sigma(\varepsilon_i) + \Sigma(\varepsilon_j)\}\right] \langle\Psi_j|, \tag{2.2}$$

where Re represents the Hermitian part and $\Sigma(\varepsilon_i)$ is derived from the GW self-energy ($\Sigma \equiv iGW$) in GW approximation (GWA). In the practical evaluation, the screened Coulomb interaction W is evaluated through the polarization function P within random phase approximation. Once the new set of ε_i and $|\Psi_i\rangle$ is obtained, it is used in the evaluation of P and W for the next iterative cycle. The details of GWA are referred to the literature [10, 11, 12].

For the QSGW calculation, we used the package *ecalj* developed by Kotani *et al.* [19, 20]. P in the QSGW calculation was performed using a 4×4×4 **k**-mesh sampling. The self-consistent calculation of QSGW was performed by an iterative procedure with a starting data constructed from DFT result. The iteration of QSGW was continued until a convergence on the maximum change in eigenvalue ε_i within 0.01 eV. Such convergence was achieved with around 10 iterations. In this work, we discussed the electronic structures based on the results of GGA, one-shot GW, and QSGW, where the one-shot GW is assigned to the first step of QSGW iterative cycles. We analyzed band dispersion curves, total and projected densities of states, and magnetic configurations.

The post-processing was done using in-house scripts with the help of parallelization implemented by GNU Parallel [21]. VESTA software package was employed to generate all crystal structure visualization [22]. The Fermi surface was produced using the XCrysDen software package [23].

3 Results and discussions

3.1 Electronic structure

The energy band dispersions of inverse B are shown in Figure 3. These figures are results for GGA, one-shot GW, and QSGW methods. In general, there are several features revealed by these energy bands. All calculations revealed half-metallic properties of $NiCo_2O_4$, where an energy gap opens at the Fermi energy in the majority spin state. For the minority spin state two bands across to the Fermi level in QSGW, whileas three bands in GGA and one-shot GW.

As shown in Figure 3, the valence band around the Fermi level consists of the three parts of oxygen orbital and two cation 3d orbitals. The oxygen part is separated from the cation parts with an energy gap, and in the majority spin state of GGA the cation parts are further separated to the occupied and unoccupied states below and above the Fermi level, respectively. In the one-shot GW, the cation part is separated into three parts in both of the majority and minority spin states. However, during the self-consistent calculation of QSGW, the cation part once separated at the one-shot GW is merged partially. As a whole property, the bandwidth of cation bands becomes narrow from GGA to QSGW.

Total and projected density of states (PDOS) obtained from GGA, one-shot GW, and QSGW are shown in Figure 4. All of PDOS display metallic behavior only at the minority spin state. The cation band around the Fermi level is distributed supposing the crystal field of the octahedral or tetrahedral site. Such a crystal field induces the energy splitting between $t_{2\text{g}}$ and e_{g} states. The DOS shape of the cation part becomes sharper from the result of GGA to those of one-shot GW and QSGW. In these GW results, the crystal field effect appears more clearly than those of

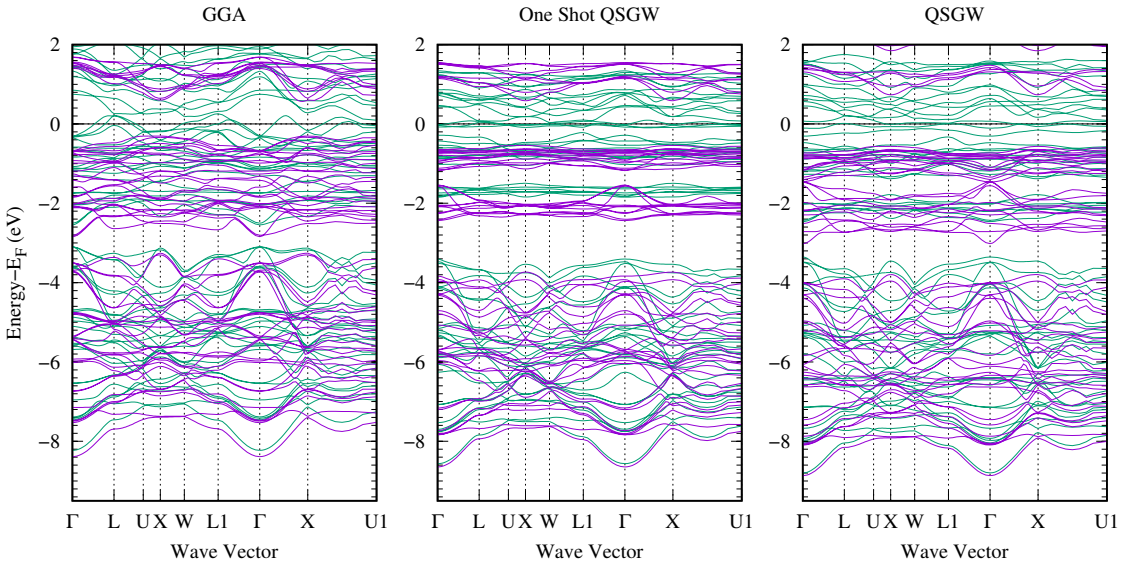

Figure 3: The energy band dispersions for $NiCo_2O_4$ with the inverse spinel type-B structure, green indicates minority spin states and magenta for majority ones. From left to right, the results of GGA, one-shot GW, and QSGW. The Fermi level presented by the horizontal line is set at zero energy.

GGA. This strongly indicates that the Coulomb interaction affected by O is taken into account more accurately through the screened Coulomb interaction W. Such effect may vary depending on the symmetry (octahedral or tetrahedral) of cation site. Particularly in the majority spin state, the conduction band above E_F in QSGW reveals a band splitting between Ni 3d and Co 3d at octahedral sites. This split may be attributed to the difference in octahedral crystal fields. The splitting of $t_{2g} - e_g$ on Ni is much larger than that on Co(oct). Our results imply that the QSGW method can provide distinct crystal fields for different cations. For the tetrahedral site [Co(tet)], effective crystal field splitting seems to be small in the results of GGA, one-shot GW, and QSGW.

The sharp PDOS of cation bands may be due to the localization of electron wave functions for the transition metals. This feature is a typical consequence resulting from the GWA. Another consequence appearing in Figure 4 is observed in the oxygen band. That band is shifted to lower energy, implying a stabilization of oxygen band in GWA.

The half-metallicity in the present work is in agreement with the previous theoretical results including the mBJ-LDA [8] and the LDA+U approaches [2, 5]. Overall DOS from the QSGW is similar to those from the mBJ-LDA and LDA+U, whereas, in the later, the oxygen band is not separated from the cation band. In regards to the cation band, the upper cation bands are shifted to the higher energies compared with the previous works mentioned above. The DOS of minority spin in the vicinity of the Fermi level is overall similar to those in the previous works but is different from them in quantitative detail.

We note some features during the self-consistent iterative cycle by comparing the PDOS between one-shot GW and QSGW. First, the degree of energy splitting from the crystal field increases in the self-consistent process. Second, as a result, the sharpness of DOS in one-shot GW becomes broad, but have never reached to the broadness of DOS-like GGA.

Figure 5 reported the total DOS and PDOS of normal spinel and inverse spinel (type A). As described before, the half-metallic structure is observed. The energy level splitting caused by the crystal field is observed like those of the inverse spinel (type B), while the Ni(tet) component is

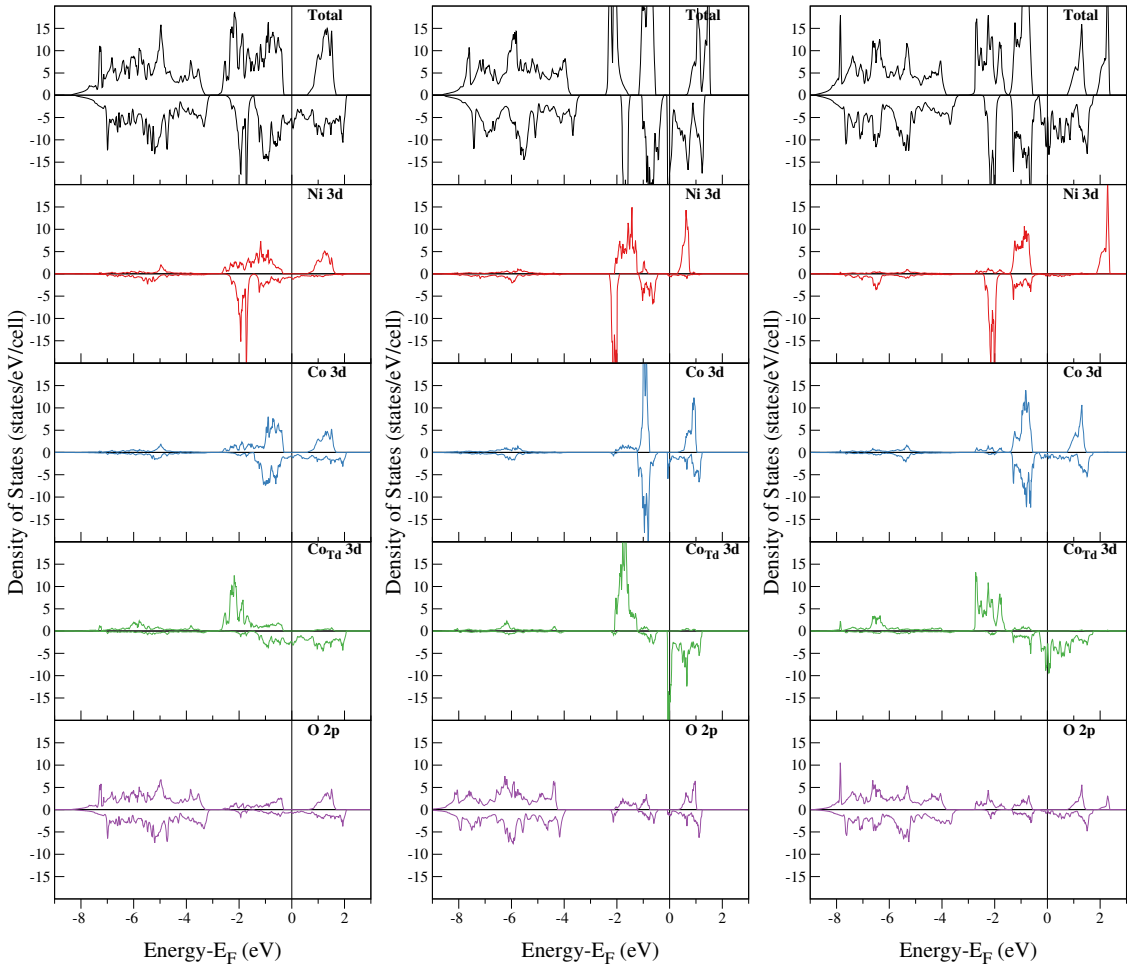

Figure 4: Total and projected densities of states (DOS) of the Ni(oct) 3d, Co(oct) 3d, Co(tet) 3d, and O 2p orbitals of inverse type B spinel $NiCo_2O_4$ for GGA, one-shot GW, and QSGW.

missing in the latter case. An important difference against the inverse type B is behavior at the Fermi level, as shown in Figure 6. Unlike the case of inverse type B, the Fermi level crosses a large peak of DOS. These behaviors strongly imply that such a metallic system has the possibility to take some form of instability. In other words, the electronic state can be stabilized further by some induction like a picture of the Jahn-Teller effect. In the view of instability, the normal spinel or inverse type A may be at a higher energy state compared with the inverse type B.

3.2 Magnetic configuration

All of the methods (GGA, one-shot GW, and QSGW) provide a net magnetization of 2 μ_B/f.u. (f.u.: formula unit.) in the inverse spinel structures of type A and type B, and also normal spinel structure. This value of net magnetization has been reported in the previous work [4]. Both inverse structures provide a ferrimagnetic arrangement, whereas the normal spinel structure exhibits ferromagnetic arrangement. However, the ferrimagnetic arrangement provided by the inverse type A has a significant difference with that of type B. This is due to the difference of cation configuration between the inverse type A and type B.

Our total magnetization is much larger than the experimental value (1.25 μ_B/f.u.) [6]. Recent experiment [2] reported that the total magnetization gradually increases to a larger value (1.84

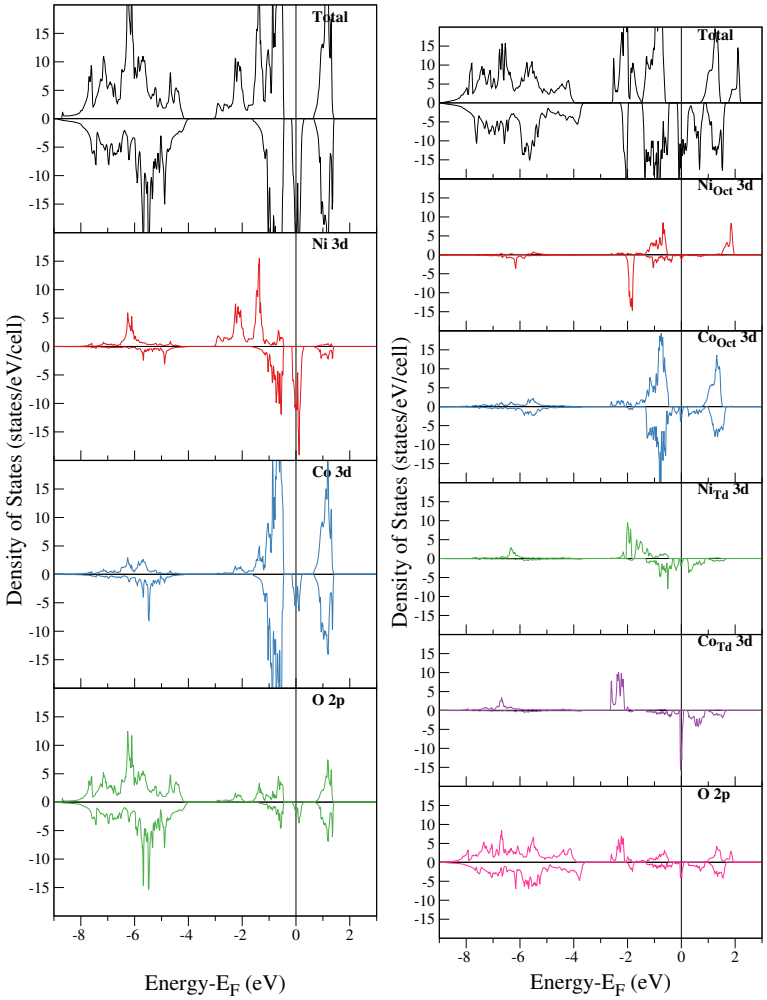

Figure 5: The total and projected densities of states of the Ni 3d, Co 3d, and O 2p orbitals of normal spinel (left) and inverse type A spinel (right) of $NiCo_2O_4$ from QSGW.

μ_B/f.u.) as the annealing time of specimen increases. This difference in the magnetization may be attributed to a disordered crystal structure in the experimental specimen.

The magnetic moment on each atom varied from GGA to QSGW, as shown in Table 2. The ferrimagnetic configuration of inverse Type B is clearly indicated. The QSGW consistently shows a larger absolute value for each atomic magnetic moment except for Co(oct). This behavior can be understood since the QSGW tends to indicate a more localized electronic state in d-orbital states. In the results of QSGW, the atomic magnetic moments of inverse B are 2.77 μ_B for Co(tet) and -1.39 μ_B for Ni. These results are comparable with the experimental data of Co(tet) 2.18 and Ni -1.49 μ_B [24] and the theoretical LDA+U data of 2.39 μ_B for Co(tet) and -1.12 μ_B for Ni [25] with U_{eff} [Ni, Co(tet) and Co(oct): 6.6, 4.7, and 6.7 eV, respectively, determined from a first-principles linear response theory]. One of the interesting results is the induction of non-negligible magnetic moment on O 2p orbitals. This contribution is estimated to be 0.40 μ_B in the formula unit, resulting from the hybridization between cation 3d and O 2p orbitals. The occurrence of magnetic moment on O atoms implies the importance of its roles for understanding the electronic structure in $NiCo_2O_4$. The moment of Co(oct) indicates a small value, which corresponds to a low spin state of Co atom.

In Table 3, magnetic moments of normal and inverse type A are reported. The ferromagnetic

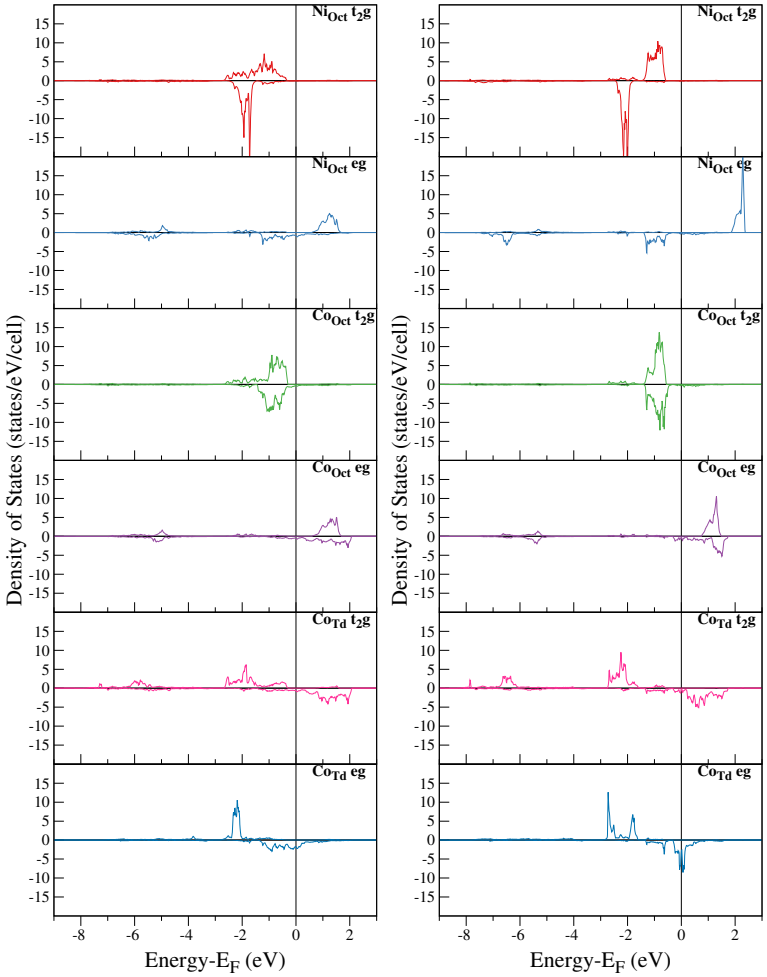

Figure 6: t_{2g} and e_g components for the projected density of states on Ni 3d and Co 3d orbitals in inverse type B spinel of $NiCo_2O_4$ from GGA and QSGW.

and ferrimagnetic configurations are indicated respectively. The moment of Ni(tet) is coupled ferromagnetically with those of Co(tet), while that of Ni(oct) is coupled antiferromagnetically. In all of the spinels investigated, the tetrahedral cation always contributes to the ferromagnetic component, while the octahedral cation contributes to the nonmagnetic or antiferromagnetic component. Additionally, the oxygen, even though the degree is small, contributes to the ferromagnetic component. Interestingly, the sum of atomic components is commonly similar among the spinel structures investigated.

3.3 Electron configuration

The atomic magnetic moment is the consequence of electron configuration at its atomic site. In the analysis of PDOS, the 3d electron configuration is tabulated for the inverse B in Table 4. These numbers of electrons are estimated within each atomic region. Therefore, the electron outside the atomic region is excluded from the value. On the comparison between the results of GGA and QSGW, several features are pointed out. First, the number is decreased at cation 3d sites and O 2p sites. Second, the number of atomic majority (minority) spin state increases (decreases) at Co_{Td} 3d and Ni 3d. Both features result in the increase of magnetic moment on Co_{Td} 3d and Ni 3d.

The electron configuration of the atom in the solid crystal may not be the best way to represent

using the ionic representation for cation elements. However, such a way is helpful to understand pictures of electronic state more deeply. As speculation, the electron configuration at the atomic state may be presented as Co(Td) 3d $(d\uparrow)^5(d\downarrow)^2$, Ni 3d $(d\uparrow)^{3.5}(d\downarrow)^5$, and Co 3d $(d\uparrow)^{3.5}(d\downarrow)^{3.5}$.

3.4 Properties at the Fermi level

The electronic states near the Fermi level consist mainly of the 3d-orbitals on Ni(oct) and Co(oct) in the majority spin state, and of the 3d orbitals on Co(tet) in the minority spin state. In Table 5, the total and partial DOS at the Fermi level (inverse type B) are reported for GGA and QSGW. The total DOS is similar to each other and the main contribution is from Co(tet). However, there are some remarkable differences in its component. The components of Ni(oct), Co(oct), and O decreases from GGA to QSGW, whileas the component of Co(tet) increases. These changes on

Table 2: Atomic and total magnetic moments (μ_B) in $NiCo_2O_4$ (inverse type B) from GGA, one-shot GW, and QSGW. Note that the averaged value is presented at O 2p.

Atom	GGA	one-shot GW	QSGW
Co(tet) 3d	2.34	2.77	2.77
Ni(oct) 3d	−0.87	−1.27	−1.39
Co(oct) 3d	0.09	0.02	0.07
O 2p	0.07	0.09	0.10
Sum in f.u.	1.81	1.86	1.86
Total in f.u.	2.00	2.00	2.00

Table 3: Atomic and total magnetic moments (μ_B) in the normal and inverse A spinels of $NiCo_2O_4$ from QSGW. Note that the averaged value is presented at O 2p.

Atom	Normal	Inverse A
Co(tet) 3d	-	2.76
Ni(tet) 3d	1.56	1.56
Ni(oct) 3d	-	−1.31
Co(oct) 3d	0.00	0.03
O 2p	0.09	0.08
Sum in f.u.	1.92	1.86
Total in f.u.	2.00	2.00

Table 4: The number of electrons in the projected orbitals in $NiCo_2O_4$ (inverse type B) from GGA, one-shot GW, and QSGW. u+d specifies the sum of up and down electrons.

Atom	GGA			one-shot GW			QSGW		
	up	down	u+d	up	down	u+d	up	down	u+d
Co(tet) 3d	4.56	2.22	6.77	4.67	1.89	6.56	4.66	1.89	6.55
Ni 3d	3.37	4.25	7.62	3.13	4.40	7.52	3.08	4.46	7.54
Co 3d	3.46	3.38	6.84	3.36	3.34	6.70	3.38	3.31	6.69
O 2p	1.74	1.67	3.40	1.73	1.64	3.36	1.74	1.64	3.37

Table 5: Total and projected DOS $N_\downarrow$ at E_F (states/eV/cell) in inverse B from GGA and QSGW. At the row of "O 2p", all O 2p contributions are included and at the row of "Sum", the summations of atomic values are reported.

$N_\downarrow(E_F)$	GGA	QSGW
Co(tet) 3d	2.45	3.50
Ni (oct) 3d	0.92	0.16
Co (oct) 3d	0.82	0.42
O 2p	0.82	0.53
Sum	5.01	4.61
Total	5.67	6.15

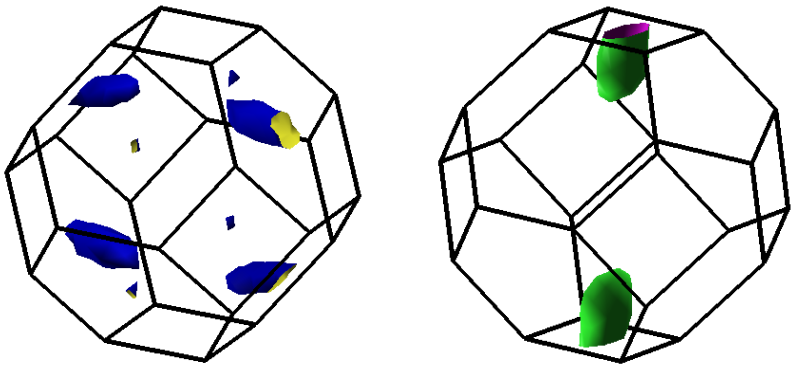

Figure 7: Fermi surfaces in inverse type B spinel of $NiCo_2O_4$ from QSGW.

the component imply a large change at the electronic state of the Fermi level.

From band dispersion curves in Figure 3, two bands cross the Fermi level at the minority spin state. As a consequence, there are two Fermi surfaces, as depicted in Figure 7. As shown, the Fermi surface is not so large that they extend to a large volume in the first Brillouin zone (**k**-space).

3.5 Comparison with LDA+U

The LDA+U approach has been used in the calculation of electronic structures for a lot of oxide materials. The necessary U_{eff} parameter is usually extracted from the empirical data. The recent work by Shi *et al.*, in which such parameters were determined in a first-principles approach, is a rare case. It can be stressed that QSGW is a non-empirical approach. Here, we point out several differences with the LDA+U results for $NiCo_2O_4$. The LDA+U provides a set of merged bands [2, 5, 25], while the QSGW provides a set of separated bands, for example, at the unoccupied state in the majority spin state (see Figure 4) and at the occupied oxygen state. On Ni(oct), the energy splitting between t_{2g} and e_g seems to be different between the majority and minority spin states.

As described, there are two energy gaps at the majority spin state around E_F which come from the $t_{2g} - e_g$ splittings on Ni(oct) and Co(oct). This consequence allows us to explain the two bandgaps extrapolated from the optical absorption spectra [3]. The edge-to-edge and peak-to-peak energy differences are 1.26 eV and 2.11 eV for Co(oct) and 2.37 eV and 3.10 eV for Ni(oct). These are comparable to the experimental gaps of 2.58 eV and 3.58 eV. Further correspondence should be verified by advanced theoretical or experimental approaches.

Despite small crystal field splitting on the tetrahedral site (see Figures 4 and 6), the QSGW result indicates two peaks in the Co(tet) e_g for both spin states. This new splitting implies some kind of effective interactions between the cations at two neighboring tetrahedral sites (separated by 3.5Å). As possible speculation, the QSGW may capture such intermediate-range interaction.

4 Summary

In summary, we have performed the first-principles investigation on electronic structure in the ferrimagnetic half-metallic inverse spinel nickel cobaltite $NiCo_2O_4$ using a QSGW method. The GWA of QSGW was found to conduct the narrower bandwidths in the band mainly consisting of the cation 3d-orbitals, implying localized wave functions in the electronic structure. The energy level splitting of t_{2g} and e_g caused by its crystal field from the PDOS results is more clearly observed than those in the GGA case. The QSGW method enables us to provide an alternative explanation for two kinds of band energy gaps from optical absorption spectra. This feature originates from the QSGW to give a distinct crystal field for different cations, particularly the splitting of $t_{2g} - e_g$ on Ni(oct) that is larger than that on Co(oct). These two gaps qualitatively make a contrast with the single gap provided by GGA and LDA+U results. The main contribution to the states at the Fermi level is found to be from Co(tet) 3d e_g orbitals. The possible states of Ni(oct) e_g, Co(oct) e_g and others are largely suppressed. As in the previous calculations of GGA and LDA+U, the electronic structure calculation from QSGW also confirms that the material $NiCo_2O_4$ is a promising candidate for spintronics application due to its half-metallicity. Unfortunately, the present calculation fails to describe an insulating/semiconducting property inherent to the $NiCo_2O_4$ at low temperatures. This new problem should be solved with a more accurate treatment in an advanced electronic structure calculation.

Acknowledgements

The computation in this work was partly performed using the facilities of the Supercomputer Center, Institute for Solid State Physics (ISSP), University of Tokyo, Japan. The authors (H.A.R., I.P., and W.R.) acknowledge the Japanese Government (MEXT) Scholarship in the Program for the Development of Global Human Resources for Kanazawa University. The authors (T.O. and M.O.) acknowledge the support from the Creation of new functional Devices and high-performance Materials to Support next-generation Industries (CDMSI), Japan.

References

[1] B. Chi , H. Lin, J. Li, N. Wang, and J. Yang, Int. J. Hydrogen Energy **31**, 1210 (2006).

[2] P. Li C. Xia, D. Zheng, P. Wang, C. Jin, and H. Bai, Phys. Stat. Sol. (RRL) **10**, 190 (2016).

[3] Y. Bitla, Y. Chin, J. Lin, C. N. Van, R. Liu, Y. Zhu, H. Liu, Q. Zhan, H. Lin, C. Chen, Y. Chu, and Q. He, Sci. Rep. **5**, 15201 (2015).

[4] G. Blasse, Philips Res. Rept. **18**, 383 (1963).

[5] K. Zhang, C. Zhen, W. Wei, W. Guo, G. Tang, L. Ma, D. Hou, and X. Wu, RSC Adv. **7**, 36026 (2017).

[6] O. Knop, K. I. G. Reid, Sutarno, and Y. Nakagawa, Can. J. Chem. **46**, 3463 (1968).

[7] P. Silwal, L. Miao, I. Stern, X. Zhou, J. Hu, and D. H. Kim., Appl. Phys. Lett. **100**, 032102 (2012).

[8] K. Dileep, B. Loukya, P. Silwal, A. Gupta, and R. Datta, J. Phys. D: Appl.Phys. **47**, 405001 (2014)

[9] D. Santos-Carballal, A. Roldan, R. Grau-Crespo, and N. H. de Leeuw, Phys. Rev. B **91**, 195106 (2015).

[10] S. V. Faleev, M. van Schilfgaarde, and T. Kotani, Phys. Rev. Lett. **93**, 126406 (2004).

[11] M. van Schilfgaarde, T. Kotani, and S. V. Faleev, Phys. Rev. Lett. **96**, 226402 (2006).

[12] T. Kotani, M. van Schilfgaarde, and S. V. Faleev, Phys. Rev. B **76**, 165106 (2007).

[13] W. Kohn and L. J. Sham, Phys. Rev. **140**, A1133 (1965).

[14] J. Otsuka, T. Kato, H. Sakakibara, and T. Kotani, Jpn. J. Appl. Phys. **56**, 021201 (2017).

[15] A. Sawamura, J. Otsuka, T. Kato, and T. Kotani, J. Appl. Phys. **121**, 235704 (2017).

[16] H. Sakakibara, T. Kotani, M. Obata, and T. Oda, Phys. Rev. B **101**, 205120 (2020).

[17] The option of spin-orbit coupling was not introduced here: T. Oda and A. Hosokawa, Phys. Rev. B, **72**, 224428 (2005).

[18] M. G. Brik, A. Suchocki, and A. Kamińska, Inorg. Chem. **53**, 5088 (2014).

[19] T. Kotani, J. Phys. Soc. Jpn. **83**, 094711, (2014).

[20] T. Kotani, H. Kino, and H. Akai, J. Phys. Soc. Jpn. **84**, 034702 (2015).

[21] O. Tange, GNU Parallel 2018, ISBN: **9781387509881** (2018).

[22] K. Momma and F. Izumi, J. Appl. Crystallogr. **44**, 1272 (2011).

[23] A. Kokalj, J. Mol. Graph. Model. **17**, 176 (1999).

[24] J. F. Marco, J. R. Gancedo, M. Gracia, J. L. Gautier, E. I. R 鱈 os, H. M. Palmer, C. Greavesc, and F. J. Berryd, J. Mater. Chem. **11**, 3087 (2001).

[25] X. Shi, S. L. Bernasek, and A. Selloni, J. Phys. Chem. C **120**, 14892 (2016).